ELSEVIER

Journal of Power Sources 84 (1999) 114–125

JOURNAL OF POWER SOURCES

www.elsevier.com/locate/jpowsour

The importance of the cathode specific interfacial area in modeling a cylindrical alkaline cell

J.J. Kriegsmann, H.Y. Cheh *

Department of Chemical Engineering and Applied Chemistry, Columbia University, 500 West 120th Street, New York, NY 10027, USA

Received 27 May 1999; accepted 4 June 1999

Abstract

Low initial cell voltage predictions from a mathematical model of a Zn/MnO_2 cylindrical alkaline cell are corrected by increasing the cathode specific interfacial area. A simplified model of the cathode region is used to estimate the initial polarization loss when the cathode specific interfacial area is changed, for a particular AA-size design and galvanostatic discharge rate. The model expression for the cathode specific interfacial area is reformulated to match the literature values for this quantity more closely. A new formulation is accepted as the revision, and the discharge time improvement is substantial with respect to the base case when simulations using the complete model are performed. The physical effects of raising the cathode specific interfacial area are analyzed. The increased discharge time leads to a localized region in the cathode that is totally depleted of zincate ion. This creates numerical problems in the cell voltage calculation.

Keywords: Alkaline batteries; Specific interfacial area; Discharge time; Zincate ion

1. Introduction

The mathematical model presented by Podlaha and Cheh [1,2] for a cylindrical Zn/MnO_2 alkaline cell has been used extensively in computer simulation of the AA-size configuration. For example, the model was applied in two studies that optimized the cell behavior by adjusting the initial cathode porosity [3] and altering the active material loading in both electrodes [4]. These four studies indicate that the model gives realistic predictions of the AA-size cell behavior. Another observation is that the model is responsive to changes in certain parameters that are considered influential with respect to the cell performance.

However, there remain certain physical discrepancies that need to be addressed prior to additional modeling of the Zn/MnO_2 system. In battery research, the cell voltage profiles are the most important results that are generated from a first principles model. In the case of the Zn/MnO_2 system, the predicted initial cell voltage is considered too low in comparison to actual cells. This tendency of the model to underpredict the operating voltage, because of a low initial cell voltage, is especially problematic for the high-rate discharge regime. In this case, a large cell current causes large activation overpotentials, so that the calculated discharge time to reach the cell cutoff voltage may be quite inaccurate because of the low value of the initial cell voltage.

The cathode region of the Zn/MnO_2 system limits the cell performance [5] in that most of the polarization losses in discharging are produced in this region because of the charge transfer and solid-state diffusion resistances. Thus, any method to correct the low predictions of the initial cell voltage should start with an analysis of the polarization losses associated with the cathode region. There are two approaches available to raise the initial cell voltage predictions [6–8]. The first technique is to vary nonphysical parameters in the governing equations of the model in an attempt to find arbitrary parameter values that raise the initial cell voltage. The second procedure is to find a rational argument for the revision of certain parameters that have a physical basis in the model, and that are related to the cell polarization.

A simplified model is developed to describe the electrochemical reaction rate in the cathode region, which pro-

* Corresponding author. Tel.: +1-212-854-4453; fax: +1-212-854-3054; E-mail: hyc1@columbia.edu

0378-7753/99/$ - see front matter
PII: S0378-7753(99)00311-0

vides for an estimation of the initial polarization loss in the cell voltage calculation. This simplified model depends largely on the single parameter, a_c, the specific interfacial area in the cathode region, under the assumption that the exchange current density evaluated at a reference condition for the cathode electrochemical reaction is invariant. Studies that focus on a small number of important parameters in a battery system are available in the literature [9,10]. The cathode specific interfacial area is a measurable, physical quantity. The results of a literature search are presented to demonstrate that the cathode specific interfacial area is too low in the complete model. A method is proposed to revise the model expression for a_c that uses the simplified description of the cathode as a guide, and simulations using the complete model are performed to identify an appropriate form of a_c. Comparisons of modeling predictions are made between simulation results using the current and revised a_c forms, so that an understanding of the physical effects of changing a_c can be obtained. The entire analysis is conducted under the assumption that a published base case AA-size configuration [1–4] is the test design being considered.

2. Simplified cathode model

A detailed overview of the Zn/MnO_2 cylindrical alkaline cell is listed elsewhere [1]. Only a brief system description is provided here. The primary Zn/MnO_2 cylindrical alkaline cell initially contains a porous Zn anode and a porous MnO_2 cathode, with a concentrated KOH aqueous electrolyte. When discharged, Zn is oxidized to form zincate ion, $Zn(OH)_4^{2-}$, which precipitates to form solid zinc oxide, ZnO, by homogeneous chemical reaction in the anode and separator regions. In the cathode, MnO_2 is reduced to form manganese oxyhydroxide, MnOOH, during the first-electron discharge of MnO_2.

It is assumed that the polarization losses in the anode region due to electrochemical reaction and ohmic effects, as well as the voltage losses in the separator region because of ohmic effects, are negligible with respect to the activation polarization losses in the cathode region [5]. The important reaction is then the single-electron reduction of MnO_2, shown as

$$MnO_2 + H_2O + e^- \rightarrow MnOOH + OH^-. \quad (1)$$

The complete cell model [1] expresses the transfer current form of this reaction as a modified Butler–Volmer equation, with additional terms that incorporate the solid-state proton diffusion. The proton diffusion term reflects the assumption of a mixed activation and diffusion control regime.

In the simplified model, the voltage loss of the entire cell is assumed to occur only because of electrochemical reaction in the cathode. The solid-state diffusion resistance in the cathode is not considered. Furthermore, the porous cathode is considered a pseudo-planar electrode, so that the transfer current is taken as a function of the cell current with no spatial dependence. For large values of $\eta_{c,sm}$, the cathode overpotential in the context of the simplified model, a Tafel form of the transfer current is used. The result is

$$j_{c,sm} = -a_c i_0 \exp\left(-\frac{\alpha_c F}{RT}\eta_{c,sm}\right). \quad (2)$$

Here, $j_{c,sm}$ is the transfer current in the cathode using the simplified model, a_c is the cathode specific interfacial area, i_0 is the exchange current density for the cathode reaction evaluated at a reference condition, α_c is the cathodic transfer coefficient for the cathode reaction, and T is the cell temperature. For small values of the cathode overpotential, a linear transfer current expression is appropriate, with the form

$$j_{c,sm} = a_c i_0 \frac{(\alpha_a + \alpha_c)F}{RT}\eta_{c,sm} \quad (3)$$

where α_a is the anodic transfer coefficient for the cathode reaction.

Since i_0 is taken as a constant, $j_{c,sm}$, a_c, and $\eta_{c,sm}$ can then be considered time-dependent quantities that do not depend on position. The transfer current is approximated by

$$j_{c,sm} = -\frac{I}{V_{cath}} \quad (4)$$

where I is the cell current and V_{cath} is the cathode volume. For a galvanostatic discharge, $j_{c,sm}$ is constant. Under this scenario of a particular constant cell current value, the relationship between a_c and $\eta_{c,sm}$ becomes apparent. A larger value of a_c will yield a value for $\eta_{c,sm}$ that is lower in absolute magnitude, and vice versa. Therefore, from the perspective of the simplified model of the cathode, if a_c is too low the result may be a prediction of $\eta_{c,sm}$ that is too large in absolute magnitude. Thus, an inspection of the model value for a_c is justified.

3. Cathode specific interfacial area

3.1. Formulation for a_c in the complete model

The model computes the cathode specific interfacial area through the assumption of identical, spherical solid reactant particles with a time-dependent outer radius denoted by r_0 [11], which increases throughout a discharge [1]. The cathode specific interfacial area is calculated from

$$a_c = 4\pi N (r_0)^2 \quad (5)$$

where N is the number density of MnO_2 particles in the cathode volume. It is seen that the only recourse to literature values occurs through r_0. Thus, the model presently does not consider the many sources of values for the specific interfacial area of electrolytic manganese dioxide (EMD), the most common battery grade form of MnO_2. The Zn/MnO_2 model assumes that the MnO_2 active material in the cathode is EMD [1].

Table 1 lists values for N and r_0^0, the initial value of the MnO_2 particle radius, for the base case AA-size design. This yields an initial cathode specific interfacial area, a_c^0, of 1200 cm^{-1}. The above expression for a_c is not readily observed in the battery literature. In the complete model formulation, a_c is a function of position in the cathode region and time.

3.2. Literature values and the relation to the Zn/MnO_2 model

A literature search is performed in order to evaluate the accuracy of the model in determining a_c. Let a_{EMD}^0 denote the literature values reported for EMD with the units of $m^2/g\text{-}MnO_2$, which indicates the specific interfacial area available at the start of discharging. The search results show that a high-end estimate of a_{EMD}^0 is on the order of 100 $m^2/g\text{-}MnO_2$ [13–24].

These values are not on a per unit electrode volume basis and must be adjusted by using

$$a_c^0 \times 10^{-4} = a_{EMD}^0 \rho_{EMD} \epsilon_{EMD}^0 \quad (6)$$

where ρ_{EMD} is the true EMD density, ϵ_{EMD}^0 is the initial volume fraction of EMD in the cathode, and the numerical factor on the left hand side is a conversion factor, because the model requires that a_c have units of cm^{-1}, for the particle surface area per unit cathode volume. The initial volume fraction of EMD, ϵ_{EMD}^0, is related to the initial cathode porosity, ϵ_c^0, through

$$\epsilon_{EMD}^0 = 1 - \epsilon_c^0 - \epsilon_G^0 \quad (7)$$

where ϵ_G^0 is the initial volume fraction of graphite, which is assumed to be 10 wt.% of the total solid material in the cathode [3,4]. The values for ρ_{EMD}, ϵ_{EMD}^0, ϵ_c^0 and ϵ_G^0 for the base case design are found in Table 1.

The above expression for the cathode specific interfacial area gives a high-end estimate of a_c^0 on the order of 10^6 cm^{-1}. This is three orders of magnitude larger than the current model value. The current value for a_c^0 is thus considered too low. Therefore, with reference to the simplified cathode model, the low value for a_c^0 may be responsible for the low initial cell voltage predicted by the complete model.

Table 1
System quantities

i_0 cathode	2.0×10^{-7} A/cm^2 [1]
α_a cathode	0.5 [1]
α_c cathode	0.5 [1]
T^0	298.15 K [1]
I	1.0 A [1]
V_{cath}	3.07 cm^3 [4]
$j_{c,sm}$	-0.326 A/cm^3
N	2.400×10^7 cm^{-3} [11]
r_0^0	20.0×10^{-4} cm [1]
ρ_{EMD}	4.370 g/cm^3 [4]
ϵ_{EMD}^0	0.626 [4]
ϵ_c^0	0.24 [1]
ϵ_G^0	0.134 [4]
$E_{ocp}(0)$	1.6 V [12]
r_s	0.45 cm [1]
r_c	0.66 cm [1]
κ^0	0.6 Ω^{-1} cm^{-1} [3]
σ_c	19.8 Ω^{-1} cm^{-1} [1]
Initial KOH concentration	0.007 mol/cm^3 [1]
Initial $K_2Zn(OH)_4$ concentration	5.3×10^{-4} mol/cm^3 [1]

3.3. Formulation to revise a_c

The simplest way to revise a_c is to slightly modify the original expression in the model. This is achieved by adding a numerical factor, k_c, in the calculation of a_c. The result is

$$a_c = k_c 4\pi N (r_0)^2 \quad (8)$$

where k_c is dimensionless. This expression appears to be an arbitrary adjustment of a_c, but the literature values for a_{EMD}^0 serve as a guide to find more realistic a_c values. This formulation to revise a_c preserves the size-change dynamics of the solid particles in the cathode.

Zhang and Cheh [25] have used an effective discharge factor in their correlations of constant load experimental discharges in order to fit the cell voltage data most accurately. The effective discharge factor itself is a pre-factor to the transfer current expression in the cathode and serves as a de facto adjustment of a_c. However, literature values for a_c when the discharge factor was used, as well as a physical analysis of the performance effect due to the discharge factor, were not included in the study. In contrast, a goal of this study is to examine the physical effects of revising a_c in the model when attempting to match the literature values of a_{EMD}^0 more closely.

4. Initial cell voltage

4.1. Simplified model

The simplified model in the cathode region is now used to estimate the initial cell voltage. This is performed by calculating the initial voltage loss in the cathode region.

For the Tafel regime, Eqs. (2) and (4) are combined to give

$$\eta_{c,sm}(0) = -\frac{RT^0}{\alpha_c F}\ln\left(\frac{I}{a_c^0 i_0 V_{cath}}\right) \quad (9)$$

Similarly, for the linear case, Eq. (3) is rearranged to give

$$\eta_{c,sm}(0) = -\frac{RT^0}{(\alpha_a + \alpha_c)F}\frac{I}{a_c^0 i_0 V_{cath}}. \quad (10)$$

In both of these equations, $\eta_{c,sm}(0)$ refers to the initial overpotential value in the cathode, and I is considered constant. The values needed to compute the initial cathode overpotential for both cases are listed in Table 1, which also gives the value of $j_{c,sm}$ for the base case design. The initial cell voltage is then calculated by

$$E_{sm}(0) = E_{ocp}(0) + \eta_{c,sm}(0) \quad (11)$$

where $E_{sm}(0)$ is the initial cell voltage calculated from the simplified model, and $E_{ocp}(0)$ is the initial open circuit potential of the cell, which is given in Table 1.

4.2. Full model

The complete Zn/MnO_2 mathematical model is referred to as the full model or complete model. The initial cell voltage calculated by the full model considers all of the relevant polarization losses at the beginning of discharge, which include contributions from the anode and separator regions, in addition to the cathode region. The initial cell voltage calculated by the full model is expressed by

$$E_{fm}(0) = E_{ocp}(0) - \eta_a(0) + \eta_s(0) + \eta_{c,fm}(0) \quad (12)$$

where $\eta_a(0)$ and $\eta_s(0)$ are the anode and separator total initial overpotentials, and $\eta_{c,fm}(0)$ is the total initial cathode overpotential for the full model. By varying k_c it is possible to perform simulations using the full model so that $\eta_{c,sm}(0)$ and $\eta_{c,fm}(0)$ can be compared. This also leads to the comparison of $E_{sm}(0)$ and $E_{fm}(0)$.

5. Secondary current distribution

When the geometrical configuration of the base case AA-size design is fixed, the current distribution in the cathode is governed by three parameters [11,26,27]. They are a dimensionless cell current, δ, a dimensionless exchange current density, ν^2, and the ratio of the matrix to electrolyte effective conductivities, γ. Since the only parameter change that is studied here involves an increase in a_c, only ν^2 will be altered. The values of δ and γ for the base case design are 3.997 and 2.807×10^2, respectively [3]. These two numbers indicate that the reaction rate in the cathode is nonuniform and skewed towards the separator/cathode interface.

The expression for ν^2 is

$$\nu^2 = \frac{(\alpha_a + \alpha_c)Fa_c^0 i_0 (r_c - r_s)^2}{RT^0}\left(\frac{1}{\kappa^0(\epsilon_c^0)^{1.5}} + \frac{1}{\sigma_c}\right) \quad (13)$$

where r_s is the anode/separator interface location, r_c is the cathode current collector location, κ^0 is a characteristic value of the electrolyte conductivity, and σ_c is the cathode effective matrix conductivity [3]. The values needed to calculate ν^2, except for a_c^0, are given in Table 1. Since a larger value is sought for a_c^0, ν^2 will increase with respect to its base case value. Increasing ν^2 will have the effect of creating a more nonuniform current distribution in the cathode.

6. Results

6.1. Overview

Simulations using the complete model are performed with different values of a_c^0, through different k_c values, using the same base case AA-size design published in earlier studies [1–4]. The operating condition is a 1.0 A discharge with a 0.8 V cutoff voltage. The numerical solution of the model has been described previously [1]. Five different cases are studied and they are summarized in Table 2. The base case design is given by $k_c = 1$. The discharge time is increased substantially as k_c is increased. The depth of discharge at the cell cutoff voltage, f_d, is also shown for each case. Greater utilization of cathode active material occurs as the discharge time is increased, due to the larger a_c values. The initial cell voltage, as predicted by the simplified and complete models, increases significantly as a_c increases.

When the initial voltage losses for the simplified model and the complete model are compared, the results are quite similar. The same is true for the initial cell voltages calculated by the full model and the simplified model. The desire to increase the initial cell voltage by raising a_c is thus validated by the simplified model, and more importantly by the complete model. The major result of the simplified model is the degree to which the initial cathodic voltage losses computed by the simplified model, $\eta_{c,sm}(0)$, match those of the complete model, $\eta_{c,fm}(0)$. These values are extremely close and appear to differ by about 50 mV for each a_c^0 value.

The simplified model underpredicts the initial cathodic voltage loss computed by the full model. For each a_c^0 value, the combined initial overpotential from the anode

Table 2
Simplified model results and simulation results from the full model

Quantity	$k_c = 1$	$k_c = 10$	$k_c = 50$	$k_c = 100$	$k_c = 1000$
a_c^0, cm^{-1}	1200	1.20×10^4	6.03×10^4	1.20×10^5	1.20×10^6
Regime	Tafel	Tafel	Tafel	Tafel	Linear
$\eta_{c,sm}(0)$, V	−0.370	−0.252	−0.169	−0.134	−0.035
$E_{sm}(0)$, V	1.230	1.348	1.431	1.466	1.565
$\eta_{c,fm}(0)$, V	−0.425	−0.307	−0.224	−0.189	−0.084
$E_{fm}(0)$, V	1.163	1.281	1.363	1.399	1.504
ν^2	5.919×10^{-3}	5.919×10^{-2}	0.2960	0.5919	5.919
t_d, h	0.700	1.006	1.150	1.189	1.278
f_d	0.277	0.395	0.451	0.466	0.500

and separator regions, as calculated by the full model, is nearly constant and is approximately 10 mV. This suggests that the initial polarization loss due to ohmic effects in the cathode accounts for the rest of the deviation between the initial cathodic overpotential values for the simplified and complete models. This additional polarization is significant, although the simplified model gives results that are surprisingly close to the full model. Therefore, the simplified model of the cathode is deemed a good approximation for the purposes of this study.

A new formulation for a_c is sought for the complete model, using a single k_c value. This is the simplest way to implement the revision. Although Zhang and Cheh [25] varied the effective discharge factor for different constant load values, the selection of a single value of k_c for the model revision is justified by the assumption of a reliable value of a_{EMD}^0 in the cell loadings, such that a_c requires an upward adjustment. However, the actual a_{EMD}^0 values that are encountered in practice are not available, so a low-end value of k_c is chosen to revise the a_c expression. The choice of a low-end k_c value ensures that the cell performance will not be overpredicted. The revised a_c expression is therefore chosen with $k_c = 50$, corresponding to $a_c^0 = 6.03 \times 10^4$ cm^{-1}. This value is in accordance with the effective discharge factor values listed by Zhang and Cheh. The rest of this study will compare predictions made by the full model for the base case and revised a_c expressions, or for the $k_c = 1$ and $k_c = 50$ simulations, respectively.

6.2. Cell voltage

Fig. 1 shows the cell voltage profiles for the five k_c values detailed in Table 2. The initial cell voltage is increased as k_c is raised, and the discharge time is substantially lengthened when k_c rises in value. It is observed that the $k_c = 50$ case captures the main adjustment in discharge time, meaning that above $k_c = 50$, the increase in cell life diminishes.

Above $k_c = 10$, voltage fluctuations appear as the cutoff voltage is approached. These occur because the longer cell life leads to the situation where a localized region of zero zincate ion concentration is encountered. Physically, this represents an interesting conceptual problem where the electrolyte reverts to a binary system in an isolated region. It is analogous to a problem treated by Hauser and Newman [28], but their results are not applicable in this study. The voltage fluctuations are considered to represent a numerical discrepancy to be addressed in future work. The zincate ion behavior is discussed in a later section.

The base case simulation with $k_c = 1$ is inferior to the other cell voltage profiles. The $k_c = 50$ case gives a 64% increase in the discharge time relative to the base case. This is a major improvement in simulated performance, and it is the result of the revision of a single, physically relevant parameter.

6.3. Transfer current

Fig. 2 shows transfer current profiles for the base case with $k_c = 1$, and Fig. 3 displays transfer current profiles for the revised case with $k_c = 50$. The profiles are shown for the cathode region. Table 2 lists the ν^2 values as k_c is raised. For $k_c = 50$, ν^2 is increased by about two orders of magnitude with respect to the base case. The current distribution is expected to be more nonuniform for the $k_c = 50$ profiles. Figs. 2 and 3 support this prediction.

The base case transfer current profiles are nonuniform, and they are large in magnitude at the separator/cathode interface. The greater nonuniformities are seen in Fig. 3 for $k_c = 50$, especially at longer times. A large reaction front penetrates the cathode to a larger extent than with the base case. Also, the reaction rate at the separator/cathode interface is lowered significantly as the discharge progresses. However, the reaction still does not penetrate the cathode near the cathode current collector, which is supported by the large ratio of matrix to electrolyte effective conductivities that is unchanged by the revision of a_c. The simplified model value of $j_{c,sm} = -0.326$ A/cm^3 is a decent characteristic value for the transfer current in both figures.

6.4. Local overpotential

Figs. 4 and 5 detail the local overpotential profiles in the cathode for $k_c = 1$ and $k_c = 50$, respectively. It is

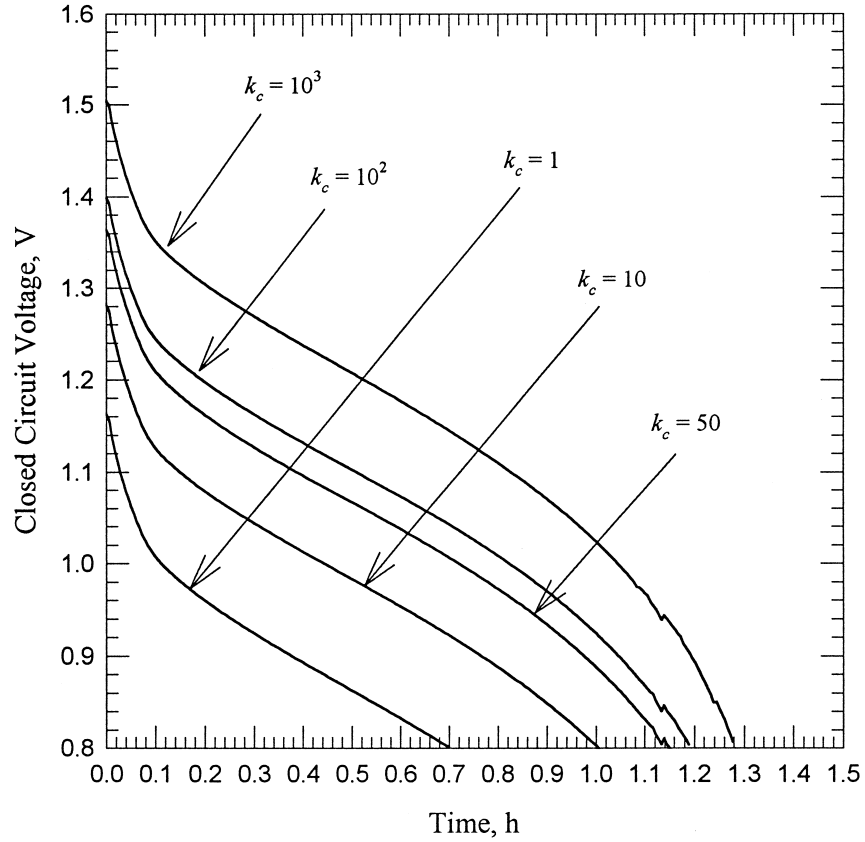

Fig. 1. Cell voltage curves with different expressions for the cathode specific interfacial area.

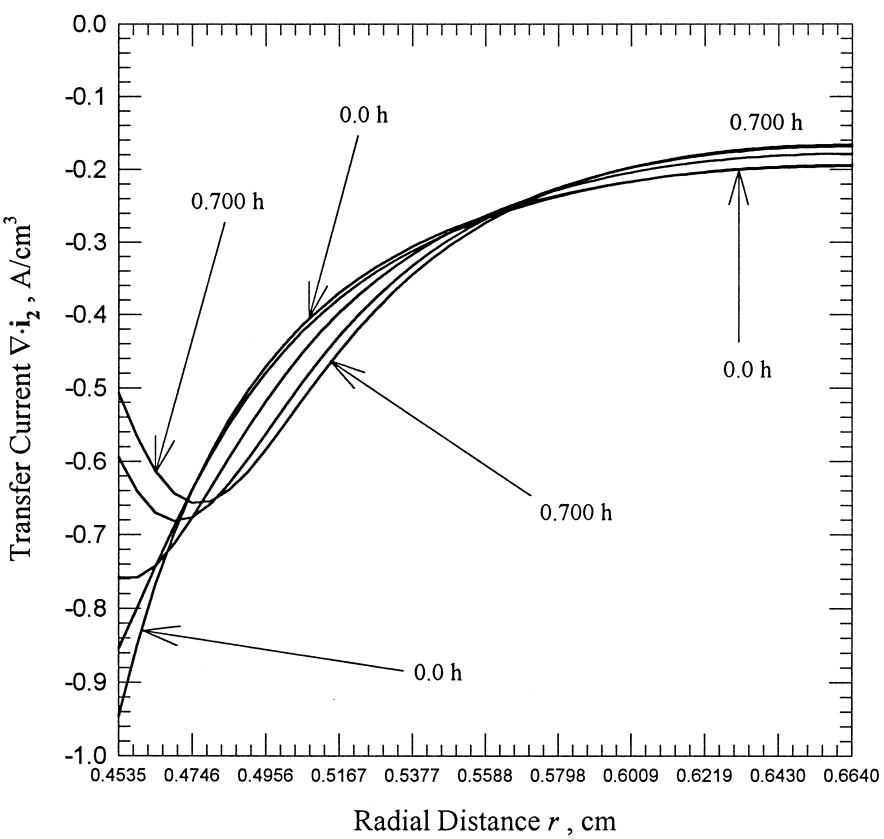

Fig. 2. Transfer current profiles throughout the cathode for the base case cathode specific interfacial area expression, with $k_c = 1$.

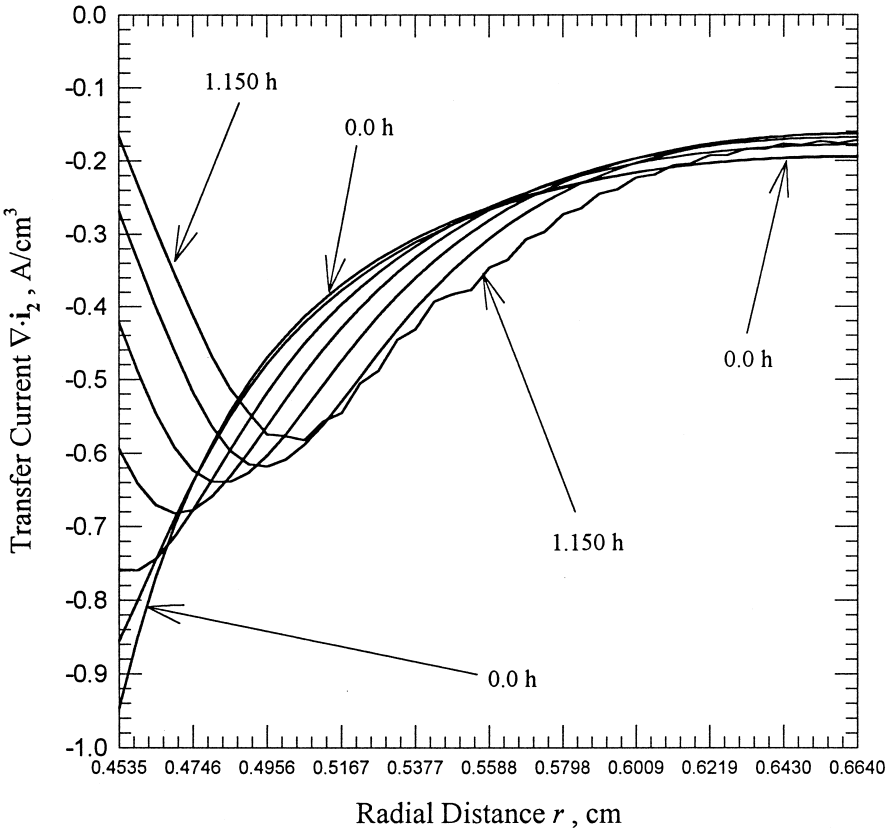

Fig. 3. Transfer current profiles throughout the cathode for the revised cathode specific interfacial area expression, with $k_c = 50$.

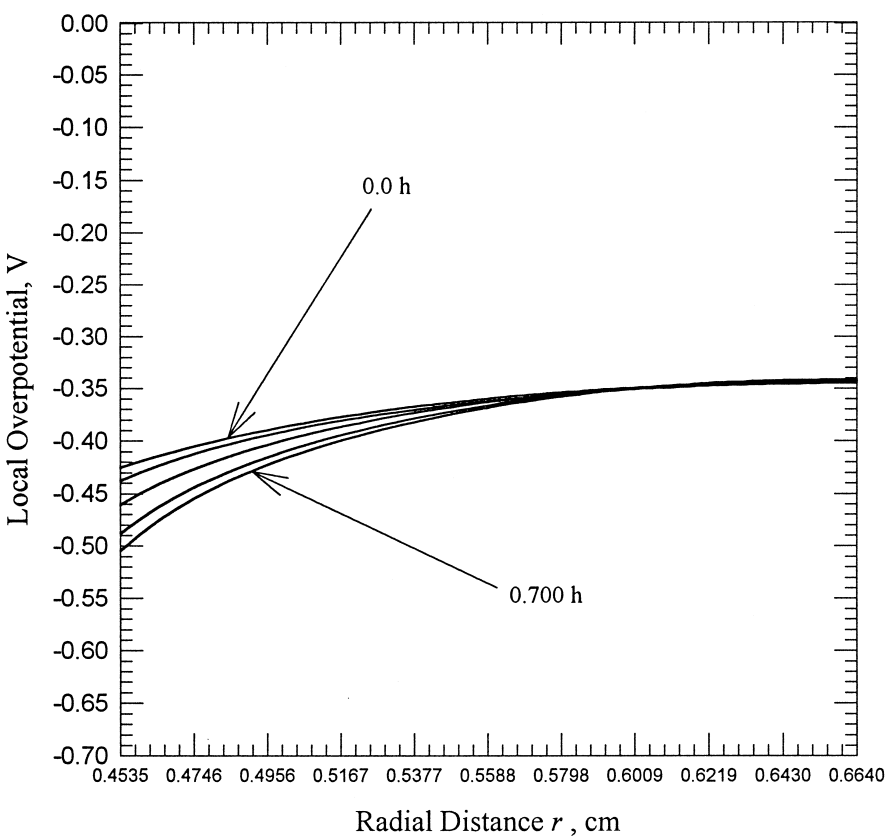

Fig. 4. Local overpotential profiles throughout the cathode for the base case cathode specific interfacial area expression, with $k_c = 1$.

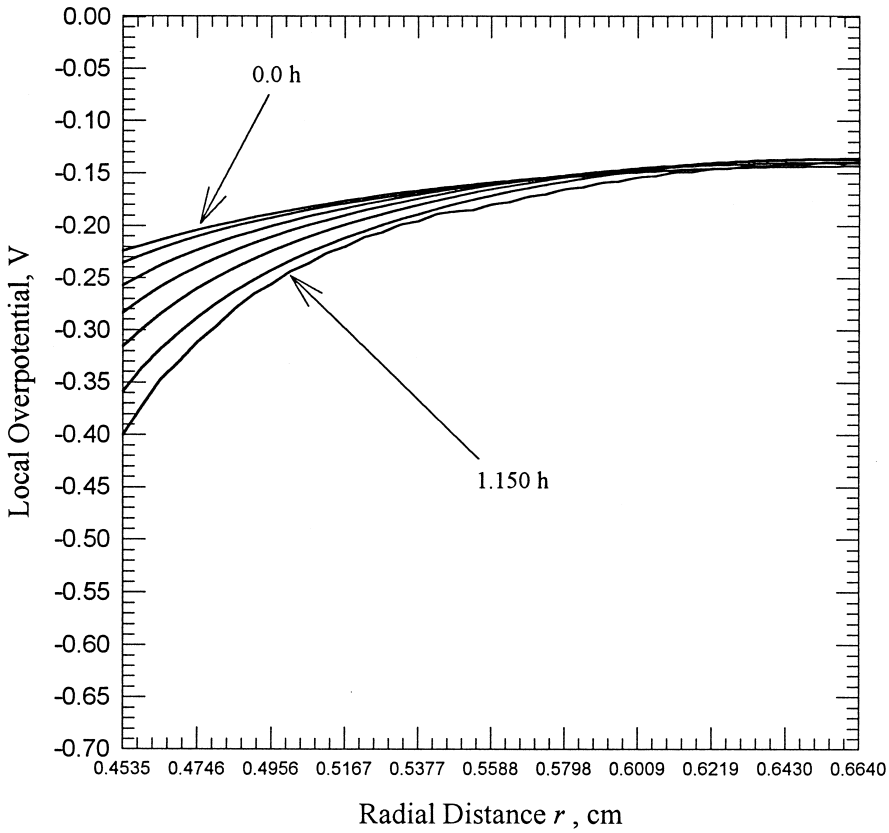

Fig. 5. Local overpotential profiles throughout the cathode for the revised cathode specific interfacial area expression, with $k_c = 50$.

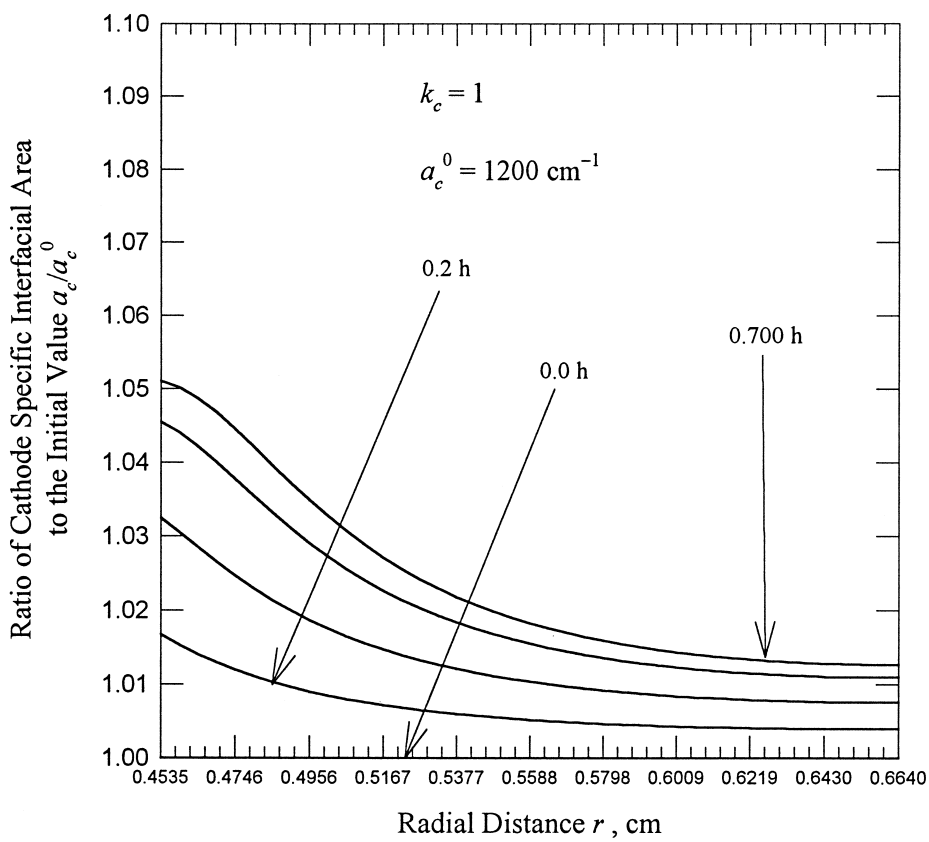

Fig. 6. Cathode specific interfacial area profiles for the base case a_c expression, with $k_c = 1$.

easily seen that the local overpotential is greatly lowered in magnitude when a_c is increased. The cell voltage calculation in the complete model depends on the local overpotential evaluated at three positions within the cell [3], where the cathode delivers the main contribution to the cell voltage loss. Thus, the lower overpotential values in the cathode directly explain the higher operating voltage, and the much longer cell life, when a_c is increased. Therefore, the appearance of lower overpotentials in the cathode is the major effect of revising a_c. A key relationship that is predicted by the secondary current distribution is seen, whereby a larger a_c leads to lower local overpotential profiles, but the reaction rate profiles become less uniform.

6.5. Cathode specific interfacial area

The profiles for a_c in the cathode for $k_c = 1$ and $k_c = 50$ are shown, respectively, in Figs. 6 and 7. The specific interfacial area increases with time in both cases. This is because r_0 increases with time [1], and the effect of r_0 is seen in Eq. (8). For the base case, the increase in a_c is limited to about 5%. The largest change occurs near the separator/cathode interface because of the larger reaction rate. The revised form of a_c with $k_c = 50$ shows similar behavior, although the more nonuniform reaction rate in the cathode leads to a slightly larger increase in a_c, which achieves a maximum of about 7% at a short distance away from the separator/cathode interface. The changes in a_c throughout a discharge are not drastic, and an argument can be made for using a constant value of a_c in the complete model.

A possible flaw in the model is the use of r_0 in the calculation of a_c. This is because r_0 describes the outer surface of a reacted solid particle that contains MnOOH in the outer shell and MnO_2 in the inner core, with the result of an overpredicted value of a_c. It may be more appropriate to use the inner radius that describes the MnO_2 shell only, which decreases throughout a discharge. However, this radius does not change very much throughout a discharge, as is the case with r_0, so that the effect of using r_0 may not be important in relation to the revised a_c formulation with the new k_c value. This also suggests that a constant a_c value may be satisfactory.

6.6. Zincate ion concentration

Figs. 8 and 9 present the zincate ion concentration profiles throughout the entire cell for the base case and revised a_c expressions, or with $k_c = 1$ and $k_c = 50$, respectively. In these figures the anode is on the left side, the separator is between the two vertical, dotted lines, and the

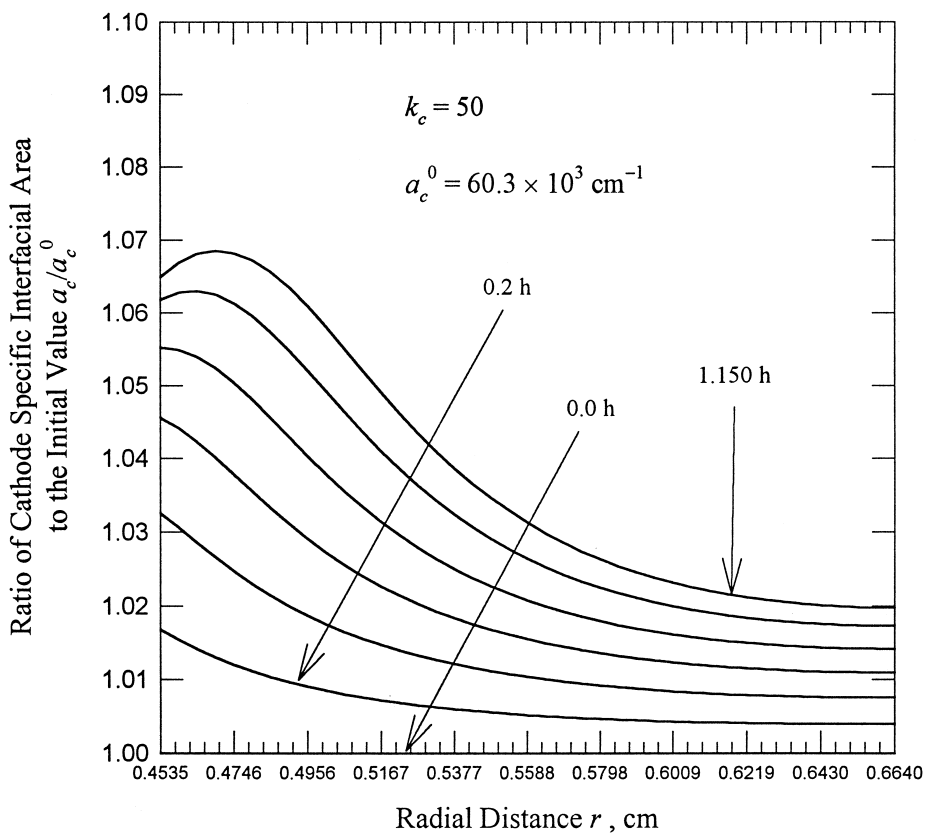

Fig. 7. Cathode specific interfacial area profiles for the revised a_c expression, with $k_c = 50$.

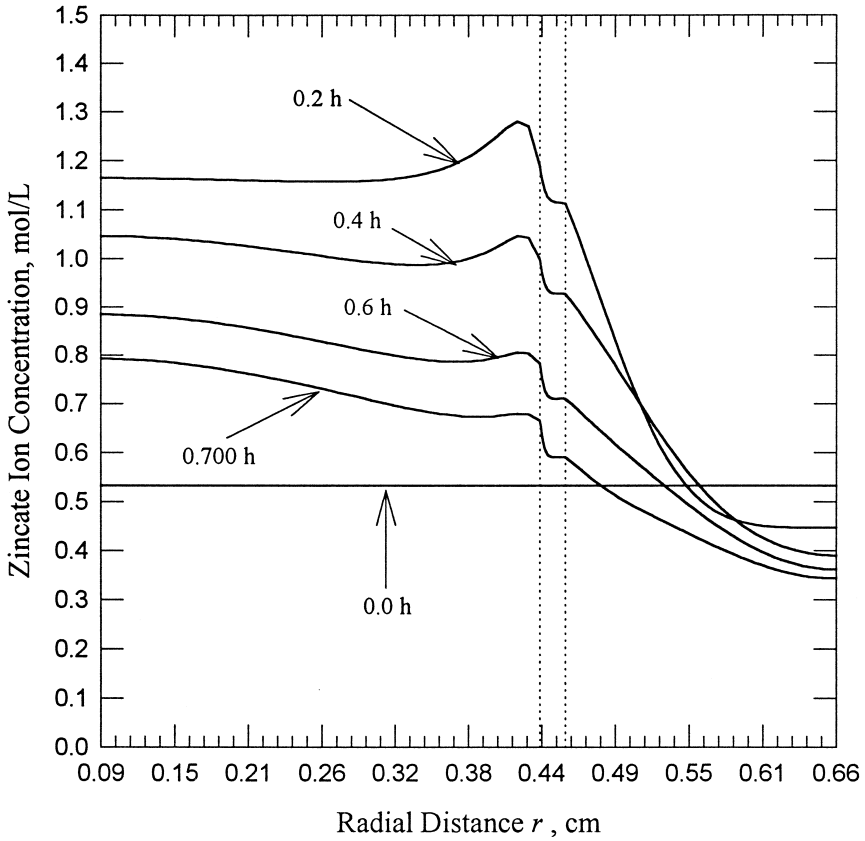

Fig. 8. Zincate ion concentration profiles throughout the entire cell for the base case cathode specific interfacial area expression, with $k_c = 1$.

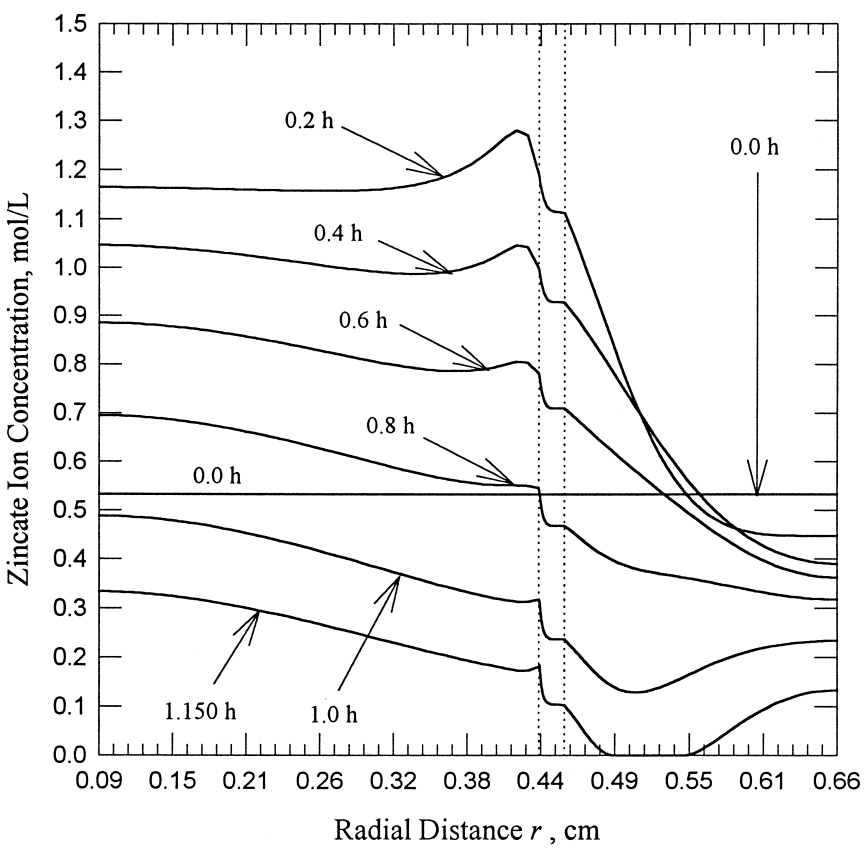

Fig. 9. Zincate ion concentration profiles throughout the entire cell for the revised cathode specific interfacial area expression, with $k_c = 50$.

cathode is on the right side. The initial KOH and potassium zincate ($K_2Zn(OH)_4$) concentrations are given in Table 1. At short times immediately after discharging begins, there is a large accumulation of zincate ion in the electrolyte. The profiles start to decrease as the discharge time increases. The profiles for both cases are nearly identical throughout the discharge time for the base case. But the much longer discharge time for the revised a_c case leads to the depletion of zincate ion in a confined region in the cathode. This is the cause of the voltage fluctuations that appear in Fig. 1.

When the zincate ion concentration is zero, the solution becomes a binary electrolyte in a localized region, yet remains a ternary electrolyte throughout the rest of the cell. The form of Ohm's law in the electrolyte phase changes when the ternary to binary electrolyte transition occurs [1]. Because of the logarithmic dependence on concentration, it is difficult to numerically implement the ternary to binary electrolyte transition without the adverse fluctuations in voltage. It is believed that the actual cause of zincate ion depletion observed here is due to the large increase in discharge time when a_c is revised, which precludes consideration of some other type of explanation. The cathode specific interfacial area does not have a direct effect on the zincate ion behavior. However, flux of zincate ion out of the cathode occurs because of migrational forces at longer times [1]. The voltage fluctuations with the revised a_c expression are unacceptable numerical inconsistencies that are to be corrected in another study.

7. Conclusions

Low initial cell voltage predictions are corrected by revising the formulation for a_c. The revision of the cathode specific interfacial area demonstrates the major effect that a single, physical parameter can have in the predictions of the Zn/MnO_2 mathematical model. A low-end adjustment to the formulation of a_c, which is supported by the literature, leads to a large simulated increase in cell life. The revised form of a_c is taken with $k_c = 50$, which gives $a_c^0 = 6.03 \times 10^4$ cm^{-1}. A simplified mathematical model of the cathode region as an idealized, spatially invariant electrode provides extremely accurate estimations of the initial polarization loss experienced by the AA-size test design as a_c is adjusted, relative to predictions made by the complete mathematical model. The revised a_c expression leads to the prediction of a more nonuniform reaction rate in the cathode, and a higher operating voltage is observed because of local overpotential profiles that are reduced in magnitude in the cathode. Finally, the revised a_c formulation leads to the depletion of zincate ion in a localized region in the cathode. This creates numerical fluctuations in the cell voltage calculation that must be corrected.

8. List of symbols

a_c	Specific interfacial area in the cathode, defined as the solid particle surface area per unit cathode volume, cm^{-1}
a_{EMD}	Specific interfacial area of electrolytic manganese dioxide as reported in the literature, $m^2/g\text{-}MnO_2$
$E_{ocp}(0)$	Initial open circuit potential of the cell, V
$E_{fm}(0)$	Initial cell voltage calculated by the full model, V
$E_{sm}(0)$	Initial cell voltage calculated by the simplified model, V
f_d	Depth of discharge at the cell cutoff voltage
F	Faraday's constant, 96,487 C/mol
i_0	Exchange current density for the cathode reaction evaluated at a reference condition, A/cm^2
I	Cell current, A
$j_{c,sm}$	Transfer current in the cathode region as calculated by the simplified model, A/cm^3
k_c	Factor used in Eq. (8) for the modified cathode specific interfacial area expression
N	Number density of MnO_2 particles in the cathode region available for electrochemical reaction, cm^{-3}
r_0	Outer radius of a solid reactant particle contained in the cathode, cm
r_c	Cathode current collector location, cm
r_s	Separator/cathode interface location, cm
R	Universal gas constant, 8.3143 J/mol K
t_d	Discharge time to reach the cutoff voltage, h
T	Cell temperature, K
V_{cath}	Cathode volume, cm^3
Greek	
α_a	Anodic transfer coefficient for the cathode electrochemical reaction
α_c	Cathodic transfer coefficient for the cathode electrochemical reaction
γ	Ratio of matrix to electrolyte effective electrical conductivities in the cathode
δ	Dimensionless cell current using cathode parameters
ϵ_i	Porosity of region i, or solid volume fraction of species i
η_a	Total overpotential in the anode region, V
η_s	Total overpotential in the separator region, V
$\eta_{c,fm}$	Total overpotential in the cathode region as calculated by the full model, V

$\eta_{c,sm}$	Total overpotential in the cathode region as calculated by the simplified model, V
κ	Electrolyte conductivity, Ω^{-1} cm^{-1}
ν	Square root of the dimensionless exchange current density in the cathode
ρ_i	Density of component i, g/cm^3
σ_c	Cathode effective matrix conductivity, Ω^{-1} cm^{-1}

Superscripts

0	Initial condition or characteristic value

References

[1] E.J. Podlaha, H.Y. Cheh, J. Electrochem. Soc. 141 (1994) 15.
[2] E.J. Podlaha, H.Y. Cheh, J. Electrochem. Soc. 141 (1994) 28.
[3] J.J. Kriegsmann, H.Y. Cheh, J. Power Sources 77 (1999) 127.
[4] J.J. Kriegsmann, H.Y. Cheh, J. Power Sources 79 (1999) 262.
[5] J.-S. Chen, H.Y. Cheh, J. Electrochem. Soc. 140 (1993) 1213.
[6] T.I. Evans, R.E. White, J. Electrochem. Soc. 136 (1989) 2798.
[7] D. Fan, R.E. White, J. Electrochem. Soc. 138 (1991) 17.
[8] P. De Vidts, R.E. White, J. Electrochem. Soc. 142 (1995) 1509.
[9] M. Doyle, T.F. Fuller, J. Newman, Electrochim. Acta 39 (1994) 2073.
[10] B. Paxton, J. Newman, J. Electrochem. Soc. 143 (1996) 1287.
[11] J.-S. Chen, H.Y. Cheh, J. Electrochem. Soc. 140 (1993) 1205.
[12] C.Y. Mak, H.Y. Cheh, G.S. Kelsey, P. Chalilpoyil, J. Electrochem. Soc. 138 (1991) 1607.
[13] W.C. Vosburgh, J. Electrochem. Soc. 106 (1959) 839.
[14] A. Kozawa, R.A. Powers, Electrochem. Technol. 5 (1967) 535.
[15] R. Huber, in: K.V. Kordesch (Ed.), Batteries, Vol. 1, Manganese Dioxide, Marcel Dekker, New York, 1974, pp. 1–240.
[16] K.V. Kordesch, in: K.V. Kordesch (Ed.), Batteries, Vol. 1, Manganese Dioxide, Marcel Dekker, New York, 1974, pp. 241–384.
[17] A. Kozawa, in: K.V. Kordesch (Ed.), Batteries, Vol. 1, Manganese Dioxide, Marcel Dekker, New York, 1974, pp. 385–520.
[18] W.J. Wruck, PhD Thesis, University of Wisconsin, Madison, WI, 1984.
[19] M. Fukuda, in: B. Schumm, Jr., M.P. Grotheer, R.L. Middaugh, J.C. Hunter (Eds.), Proceedings of the Symposium on Manganese Dioxide Electrode Theory and Practice for Electrochemical Applications, PV 85-4, The Electrochemical Society Proceedings Series, Pennington, NJ, 1985, pp. 180–190.
[20] K. Takahashi, Y. Nakayama, in: B. Schumm, Jr., M.P. Grotheer, R.L. Middaugh, J.C. Hunter (Eds.), Proceedings of the Symposium on Manganese Dioxide Electrode Theory and Practice for Electrochemical Applications, PV 85-4, The Electrochemical Society Proceedings Series, Pennington, NJ, 1985, pp. 208–221.
[21] A.V. Fraioli, in: B. Schumm, Jr., M.P. Grotheer, R.L. Middaugh, J.C. Hunter (Eds.), Proceedings of the Symposium on Manganese Dioxide Electrode Theory and Practice for Electrochemical Applications, PV 85-4, The Electrochemical Society Proceedings Series, Pennington, NJ, 1985, pp. 342–368.
[22] I. Tanabe, N. Miyamoto, in: B. Schumm, Jr., M.P. Grotheer, R.L. Middaugh, J.C. Hunter (Eds.), Proceedings of the Symposium on Manganese Dioxide Electrode Theory and Practice for Electrochemical Applications, PV 85-4, The Electrochemical Society Proceedings Series, Pennington, NJ, 1985, pp. 493–524.
[23] B. Schumm, Jr., G.W. Mellors, in: B. Schumm, Jr., M.P. Grotheer, R.L. Middaugh, J.C. Hunter (Eds.), Proceedings of the Symposium on Manganese Dioxide Electrode Theory and Practice for Electrochemical Applications, PV 85-4, The Electrochemical Society Proceedings Series, Pennington, NJ, 1985, pp. 525–538.
[24] K.E. Anthony, J. Ostwald, in: B. Schumm, Jr., M.P. Grotheer, R.L. Middaugh, J.C. Hunter (Eds.), Proceedings of the Symposium on Manganese Dioxide Electrode Theory and Practice for Electrochemical Applications, PV 85-4, The Electrochemical Society Proceedings Series, Pennington, NJ, 1985, pp. 628–649.
[25] Y. Zhang, H.Y. Cheh, J. Electrochem. Soc. 146 (1999) 850.
[26] J. Newman, W. Tiedemann, AIChE J. 21 (1975) 25.
[27] M. Doyle, T.F. Fuller, J. Newman, J. Electrochem. Soc. 140 (1993) 1526.
[28] A.K. Hauser, J. Newman, J. Electrochem. Soc. 136 (1989) 3319.